ESTIMATING YIELD AND DEPTH OF BURIAL FROM *Rg*

Jessie Bonner[1], Aaron Ferris[1], Robert Reinke[2], and Elizabeth Lenox[2]

Weston Geophysical Corporation[1] and the Defense Threat Reduction Agency[2]

Sponsored by the Air Force Research Laboratory[1] and the Defense Threat Reduction Agency[2]

Award No. FA8718-09-C-0051

ABSTRACT

We have examined the feasibility of using short-period, fundamental-mode surface waves (*Rg*) to estimate the yields and depths of burial (DOB) of small chemical explosions recorded at local distances. *Rg* and other surface wave arrivals were recorded from the HUMBLE REDWOOD I and II (HR I and II) experiments (Foxall *et al*., 2008, 2010). The HRI and II experiments were comprised of ten 656 kg ANFO (539 kg TNT-equivalent) charges detonated between 5 m height of burst (HOB) and 10 m DOB and three additional blind yield and DOB shots. The experiments were conducted in and above the dry alluvium of Kirtland AFB, NM near the eastern margin of the Albuquerque Basin, and were recorded by extensive local seismic and acoustic networks.

Our *Rg* analysis technique includes developing a velocity model using inversion of *Rg* group velocity dispersion data and estimating a frequency-dependent Q model for *Rg.* The velocity and Q models developed for the region around the HUMBLE REDWOOD test site show two distinct regions separated by the Hubbell Springs normal fault. To the west of the fault (graben), upper crustal *Rg* velocities are slow (0.3 to 0.7 km/sec) and are indicative of dry alluvium. East of the fault (horst), the *Rg* velocities are faster (0.8 to 2 km/sec) and are representative of more competent bedrock (limestone). Similarly, the Q is lower (2 to 15) to the west of the fault than to the east (15 to 50). The fault also acts as an intense scattering mechanism for *Rg*. The *Rg* wave packets west of the fault are easy to identify and process, while, east of the fault, the fundamental model is not easily differentiated from scattered waves.

Next, we correct the observed spectral amplitudes to 1 km, estimate synthetic spectral amplitudes for isotropic explosions, and determine the best fit moment to the observed *Rg* spectral amplitudes. For the ten 539 kg shots, we estimate isotropic moments ranging between 2E10 (5 m HOB) to 1.5E11 N-m (10 m DOB). Finally, we estimate a range of DOB and yields that fit these moments based on the Denny and Johnson (1991; DJ91) explosion source model. The yield estimates for the estimated moments range from 23 to 508 kg. The wide range in yield estimates (e.g., factor of 22) for these equivalent yield explosions (539 kg) is due to venting effects for the shallow buried and above-ground explosions. We attempt to define corrections for confinement effects based on combinations of the explosion characteristics (e.g., emplacement depth, cavity radii, damage, and elastic radii). We determine that correcting the observed moments by a factor defined by the emplacement depth divided by the cavity radius significantly reduced the error in the yield estimates. This correction changes the estimated yield of a surface explosion from 23 kg to 726 kg, which differs from the true yield by less than a factor of 2. We also examine corrections to the seismic moments for the shallow buried, surface and height of burst shots based on crater parameters determined by means of digital photogrammetry.

OBJECTIVES

Short-period fundamental mode Rayleigh waves (*Rg*) are often recorded at local distances from explosions. The appearance of the phase ranges from an easily-identified Airy phase to a complex waveform scattered by topography or geophysical structure. At local distances, *Rg* is often the largest arrival observed on seismograms, and its presence is indicative of shallow source depth. Thus the phase is often observed from single-point explosions, delay-fired explosions, and shallow earthquakes. While the phase rarely propagates to regional distances due to rapid attenuation and scattering, *Rg* has been used to better understand source phenomenology (Patton et al., 2005), *S*-wave generation (Myers et al., 1999), depth estimation (Kafka, 1990; Anderson et al., 2007), and velocity and attenuation model development (Saikia et al., 1990). Adushkin (2001) demonstrated the ability to use *Rg* amplitudes at near-regional distances to provide seismically-estimated yields that were within 20% of the true yields for Semipalatinsk underground explosions. The objective of this one year feasibility study is to determine if small explosion yields can be estimated reliably using short-period surface waves, including *Rg*.

RESEARCH ACCOMPLISHED

We developed a method that examines the tradeoffs between depth of burial (DOB), *Rg* excitation, and yield estimation. Our new technique includes 1) development of a velocity and attenuation model using inversion of *Rg* group velocity dispersion data, 2) propagation of synthetics with isotropic moments through these models to determine the best fit to the observed *Rg* spectral amplitudes, and 3) estimation of a range of DOB and yields that fit these moments using the Denny and Johnson (1991) explosion source model and near-source material properties.
m
We provide an example of this yield estimation method using data recorded from the HUMBLE REDWOOD (HR) I and II experiments (Foxall et al., 2008 and 2010) conducted at Kirtland Air Force Base in Albuquerque, NM (Figure 1). The HR I experiment was comprised of seven 1450-lb ANFO charges detonated at various heights of burst (HOB) and DOB. HR II included three additional 1450-lb detonations as well as three blind yield and DOB shots. Both sets of experiments were conducted in and above the dry alluvium of Kirtland AFB, NM near the eastern margin of the Albuquerque Basin, and were recorded by extensive local seismic and acoustic networks. The complete HUMBLE REDWOOD data set ranges from fully contained to no-crater height of burst shots and covers almost an order of magnitude in explosive yield.

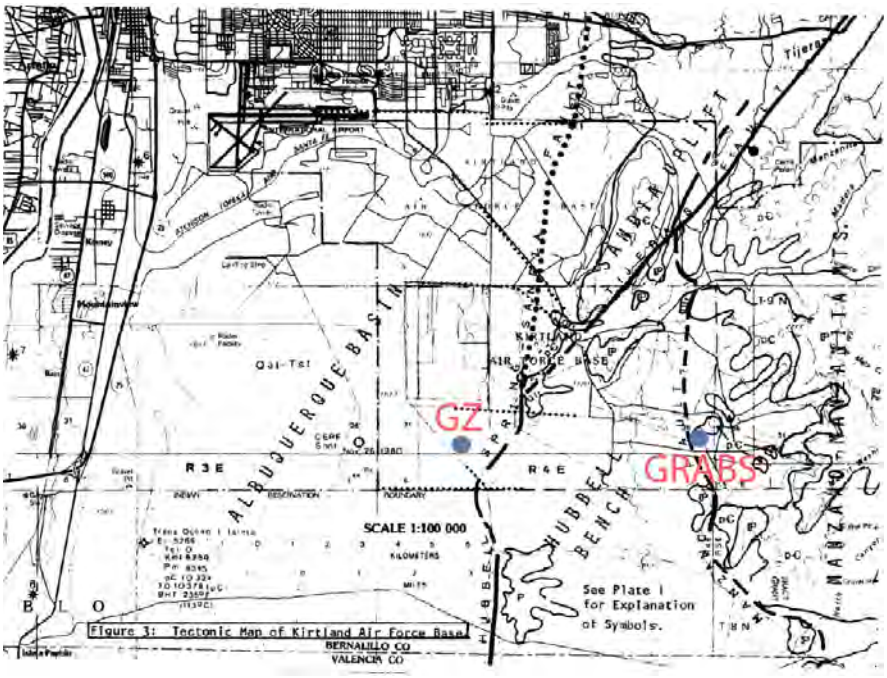

Figure 1. Geologic map showing the location of the Hubbell Springs fault approximately relative to the HR I and II test sites (GZ and GRABS). Map from Grant (1981).

Velocity and Attenuation Model Development

***P*-Wave Model.** The first step in our yield estimation method is the development of velocity and attenuation models for the explosion site and propagation path. For the *P*-wave model, we used a trial-and-error method to estimate the 2D velocity structure (Figure 2). The model was developed from *P* travel-times of two explosions recorded by 100 Texan instruments deployed between the GZ and GRABS shot locations (Figure 1). Using refraction modeling techniques and an eikonal ray tracer (Hole and Zelt, 1995), we forward modeled the travel times and adjusted the model to best match the observations. We limited the model to 5 adjustable units to simplify the trial-and-error procedure. With this simple model we were able to capture the main features of the travel-time curves for both the GZ and GRABS shots. Our modeling exercise revealed that the location and orientation of the Hubbell Springs fault was of particular importance to the quality of the travel-time fits, especially with regards to the position of the breaks observed in the travel-time curves. West of the fault, the travel-times required slow *P*-wave speeds (1-2.4 km/s) and east of the fault faster velocities were required (~3.8 km/s). A more refined model using a tomographic inversion procedure with interfaces and a larger dataset is under development.

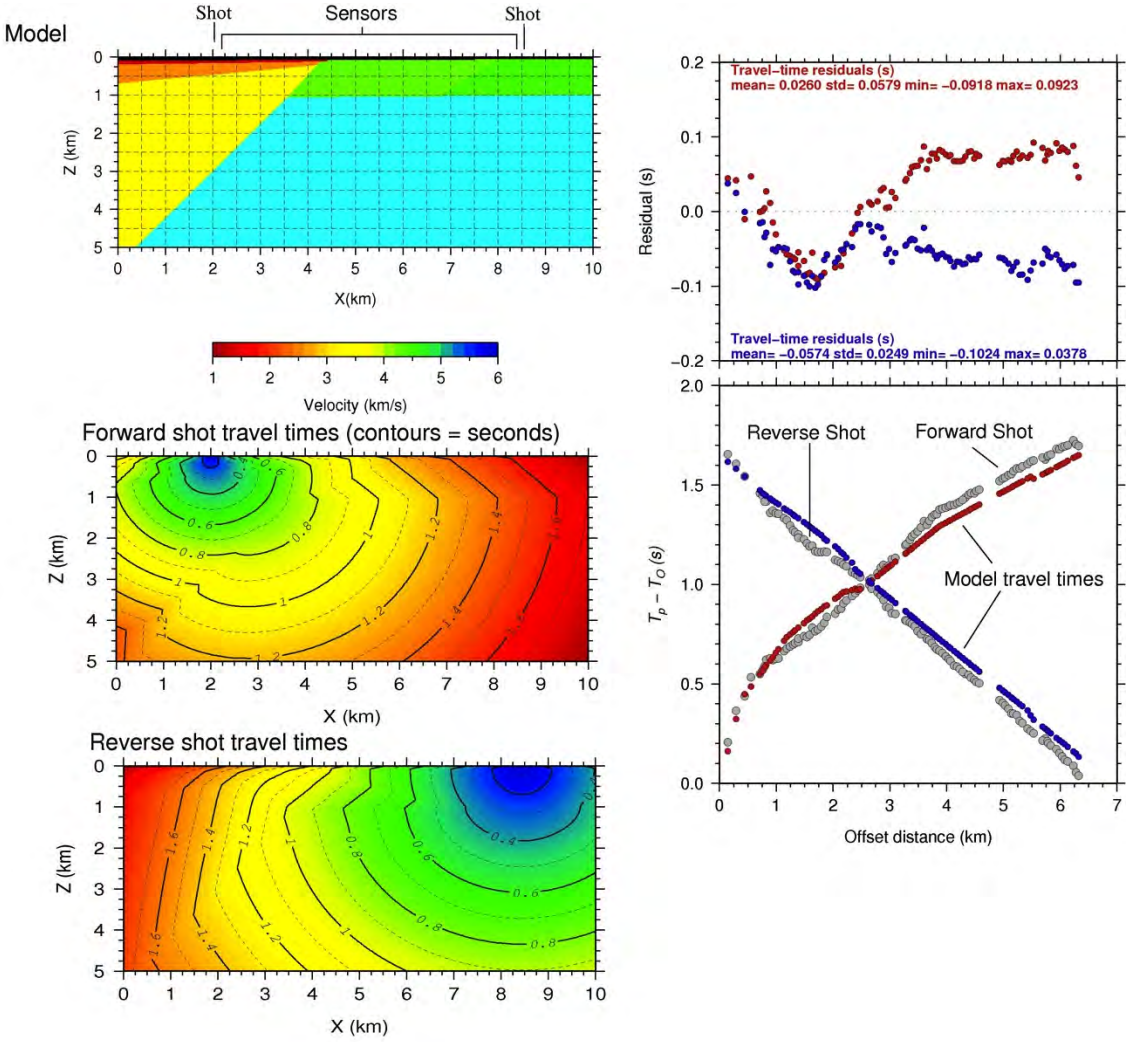

Figure 2. Development of an initial *P*-wave velocity model using first arrival forward and reverse ray tracing through the Hubbell Springs fault. (Top left) *P*-wave model showing the forward/reverse shot locations and the positions of the sensors. (Bottom left) 2D eikonal travel-times for the forward and reverse shot. (Top right) Comparison of the travel-time residuals between the forward shot (red) and reverse shot (blue). (Bottom right) Observed (gray) and modeled travel-time curves.

***S*-Wave Model.** One of the advantages of using short-period, fundamental mode surface waves to develop *S*-wave velocity models is that inversion of the group velocity dispersion curves and attenuation decay estimates for structure requires no knowledge of source properties. Examination of the group velocity dispersion curves, measured using multiple filter analyses and phase match filtering (Dziewonski *et al*., 1969; Herrin and Goforth; 1977; Herrmann, 2010) for the HR I and II shots showed two distinct velocity ranges (Figure 3). Up to 1.8 km east of ground zero (GZ), the velocities observed at periods between 0.1 and 1 second range from 0.3 km/sec to 0.8 km/sec. These values are indicative of the dry alluvium that comprises these paths and GZ in the Albuquerque Basin. At approximately 2 km east of GZ, the Hubbell Springs Fault (Grant, 1981) has an upthrown block (e.g., the Hubbell Bench) comprised of limestone and granite overlain by thin alluvial deposits. The fault rapidly scatters the surface wave energy rendering identification and measurement of *Rg* more difficult than on the western stations. Figure 3 (right) shows the dispersion curves for paths from an explosion at a different test site (called GRABS) located 7 km east of GZ with paths confined to the horst block of the Hubbell Springs Fault. On the upthrown side of the fault, the velocities range from 0.7 km/sec to 2 km/sec at periods between 0.1 to 1 seconds.

Q Model. The method used to estimate Q_{Rg} is based on Patton et al. (2005) wherein R_g amplitudes are assumed to spread geometrically as $\Delta^{-1/2}$, where Δ is epicentral distance. After correcting for geometric spreading, the decay of R_g amplitude with distance is attributed to an attenuation operator γ. Regressions of the *Rg* amplitude decay with distance are used to estimate γ at each period (Figure 4). The estimates are converted to Q_{Rg} (Figure 4) using the group velocities shown in Figure 2. The apparent Q_{Rg} estimates on the basin side of the Hubbell Springs fault range between 5 and 20, while the estimates are slightly higher (20-50) on the Hubbell Bench. We use the Q estimates to correct the observed *Rg* spectra back to a reference distance (e.g., 1 km in Figure 5).

Inversion for Structure. The final stage in the velocity model development is to input the preliminary *P*-wave velocity model (Figure 2), the *Rg* dispersion curves (Figure 3), and the attenuation decay constants (Figure 4) into a joint inversion for velocity and attenuation structure at depth. We used the Stump (1987) model as the starting model in the inversions and then performed a least squares inversion for *S*-wave velocity (*P*-wave velocity fixed) and *Q* using the codes of Herrmann (2010). The resulting velocity and attenuation structures (Figure 6) show that only a slight modification of the Stump (1987) model results in a good fit to the observed dispersion west of the Hubbell Springs fault. Because the velocities are slow in this basin, we are unable to resolve the structure below 250 meters. To the east of the fault, the velocities are faster and resolution is achieved to a depth of approximately 1 km.

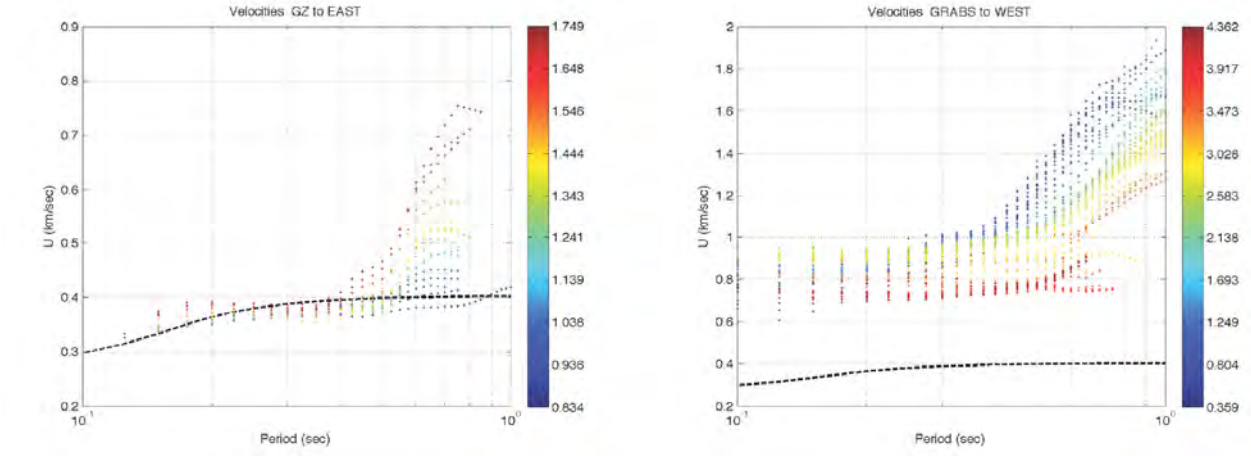

Figure 3. *Rg* group velocity dispersion curves for paths west (left) and east (right) of the Hubbell Springs fault. The colors represent distance (km) from the shot point. The dashed line represents predicted group velocity dispersion based on a velocity model developed by Stump (1987) for a location near the HR test site.

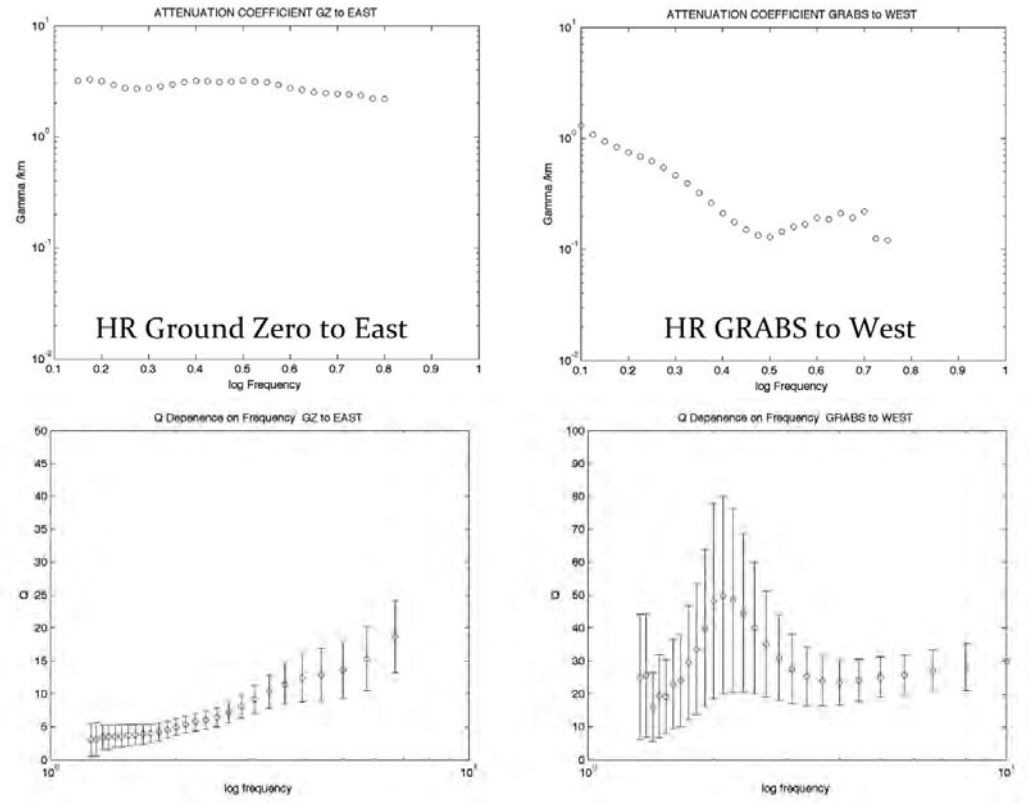

Figure 4. (Top) Attenuation γ (gamma) versus log frequency for stations west (left) and east (right) of the Hubbell Springs Fault. (Bottom) Conversion of the γ estimates to Q_{Rg}.

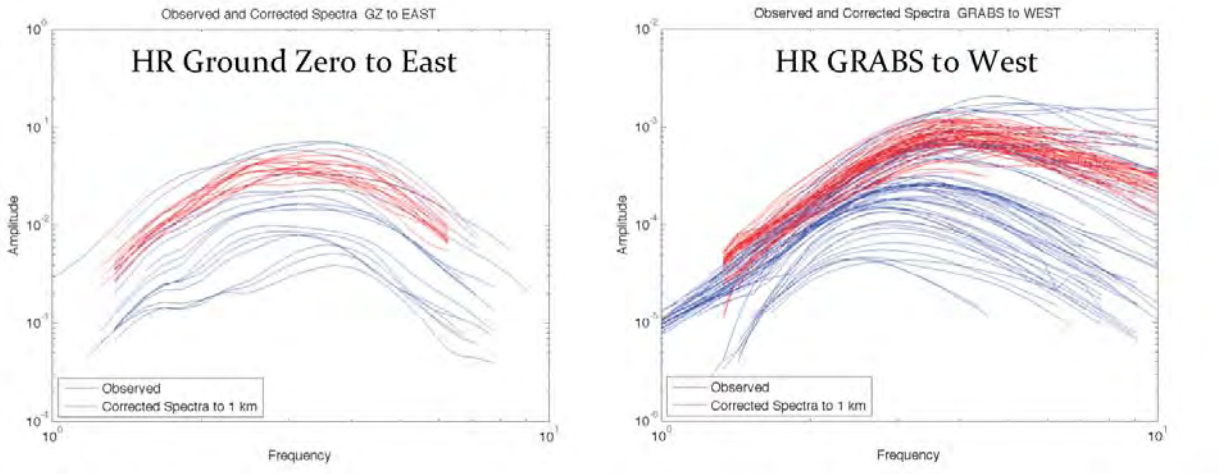

Figure 5. Observed *Rg* spectral amplitudes (blue) corrected for spreading and attenuation (red) to reference distance of 1 km for paths west (left) and east (right) of the Hubbell Springs fault.

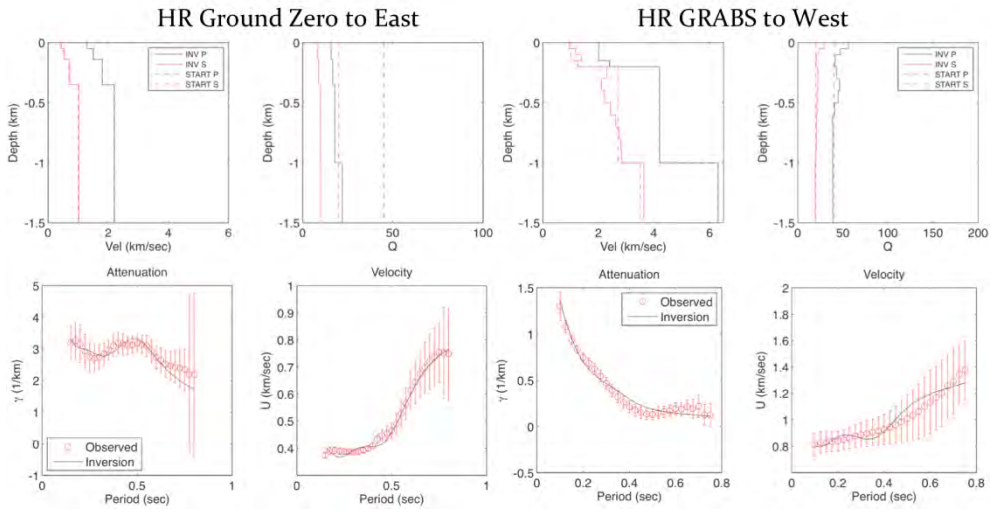

Figure 6. Inversion results. (Top) Inverted (solid lines) and starting (dashed) velocity and apparent Q models with depth obtained from the joint inversion of group velocity dispersion curves and attenuation decay constants. (Bottom) Fit of the observed dispersion and attenuation data (red) to the predictions (black) from the inverted models.

Estimating Seismic Moments for the Explosions

The next step in the procedure is to fit the corrected *Rg* spectral amps (Figure 4) with synthetic spectra from an isotropic explosion with known moment. At the publication time of this paper, we have only completed this modeling for stations west of the Hubbell Springs fault. Using the inversion model for the basin to the west of the fault (Figure 6), we generated isotropic synthetics of various moments ($M_{xx}=M_{yy}=M_{zz}$ and all off-diagonals=0) for a near surface explosion (1 m depth). We find the isotropic moment that provides the best fit to our data. Typically, we try to find the moment that fits the longer period parts of the *Rg* spectra (e.g., 0.5-3 Hz) as the calculated Green's functions do not consider corner frequency effects or secondary effects such as CLVD. Figure 7 shows the observed spectral amplitudes for ten 1450-lb HRI and II explosions at depths ranging from 10 m DOB to 5 m HOB compared to spectral amplitudes of synthetics with isotropic moments of 1E10 N-m, 1E11 N-m, and 1E12 N-m. The best fitting moments are also plotted as a function of scaled HOB.

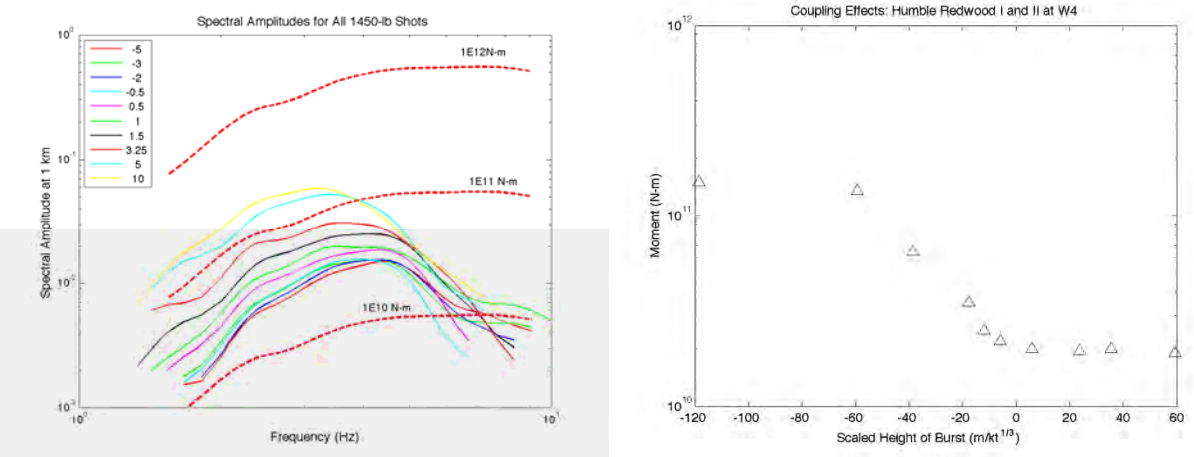

Figure 7. Moment estimation for the HUMBLE REDWOOD shots. (Left) *Rg* spectral amplitudes corrected to 1 km for ten 1450-lb shots at various HOBs/DOBs compared to synthetic *Rg* (dashed lines) with isotropic moments ranging from 1E10 N-m to 1E12 N-m. (Right) Estimated moments versus scaled Height of Burst (sHOB).

Conversion of Moment to Yield

We use Denny and Johnson (D&J; 1991) to estimate the yield of the explosion based on the estimated moment. Denny and Johnson developed a model for the measured seismic moment (M_o) of explosions:

$$M_o = \frac{1}{311} M_t P_o^{0.3490} 10^{-0.0269GP}, \qquad (1)$$

where GP is gas porosity and P_o is overburden pressure ($P_o=\rho gh$). M_t is the theoretical moment and is defined as:

$$M_t = \frac{4}{3}\pi\rho\alpha^2 R_c^3, \qquad (2)$$

where α is the P-wave velocity and R_c is the cavity radius estimated by:

$$R_c = \frac{1.47x10^4 Y^{\frac{1}{3}}}{\beta^{0.3848} P_o^{0.2625} 10^{0.0025GP}}. \qquad (3)$$

From the equations above, we note that the measured moment for explosions in the D&J model depends on the P-wave and S-wave (β) velocities and yield (Y).

We used D&J to investigate the relationship between yield and depth of burial using the HUMBLE REDWOOD seismic moment estimates (Figure 8). We used the densities and velocities from the upper layers in our inverted velocity model for GZ. We assumed a gas porosity of 10% based on geotechnical data for alluvium. The observed moment for the 1450-lb ANFO (1189-lb TNT equivalent) 10 m DOB event is presented as a white line in Figure 8, overlain on a color map of seismic moment as a function of depth of burial and yield. These plots show the importance of shot emplacement media, in addition to expected depth of burial, on the surface wave moments generated from explosions with similar yields. Our estimated yield at the explosion DOB matches very closely to the true yield of the explosion (white star). The shot at 10 meters DOB was detonated at the greatest depth, however HR II-1 (blind yield) had a greater scaled DOB. As the events become underburied or were detonated above ground, our technique grossly underestimates the yields of the explosions.

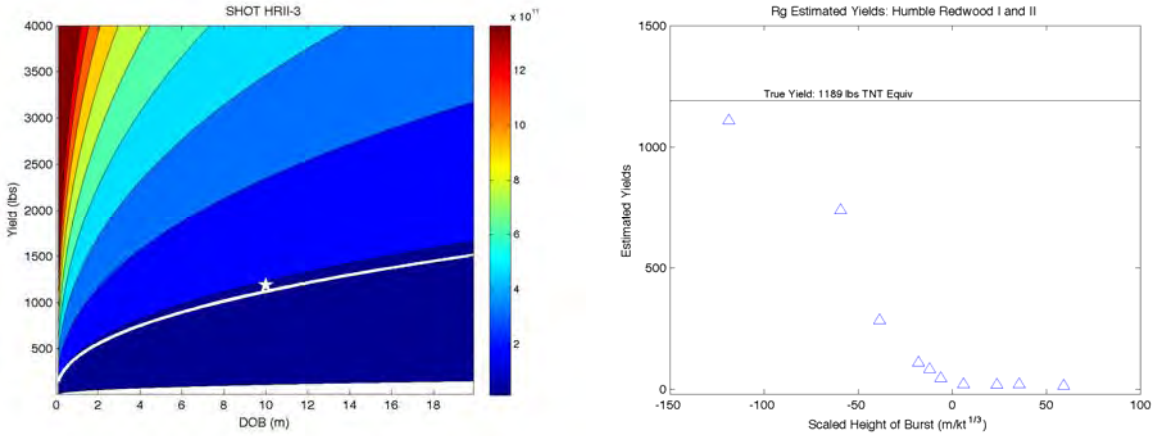

Figure 8. (Left) Moment to yield conversion using D&J and the seismic moment estimate from the *Rg* spectra of the 10 m DOB HUMBLE REDWOOD shot. The white line corresponds to 1.5E11 N-m. (Right) Yield estimates for all 1189-lb HR shots as a function of sHOB.

There is currently no explosion source model that incorporates venting, cratering, or atmospheric coupling effects when predicting the seismic moment. We are currently addressing this knowledge gap by developing a correction based on phenomenological constraints for explosions. An explosion typically has a cavity radius (R_c), a damage radius (R_d), and an elastic radius (R_{el}). We have investigated many different combinations of these terms to explain the change in seismic moment as a function of DOB/HOB due to the non-linear effects of venting and cratering. The three terms we have determined to work best at improving the yield estimation include moment correction factors based on:

$$\frac{DOB}{R_c}, \frac{DOB}{\sqrt{R_d}}, \text{ and } 1\text{-}\frac{V_1}{V_2}. \quad (4)$$

where V_1 is the volume of a 30° cone of damage above the working point where the height of the cone is R_d-DOB. V_2 is also the volume of a similar cone of damage where the height is R_d. Figure 9 shows the estimated yields when these corrections are applied to the moment-to-yield conversion. Most of the estimated yields are now within a factor or 2 or 3 of the true yields of these HUMBLE REDWOOD explosions.

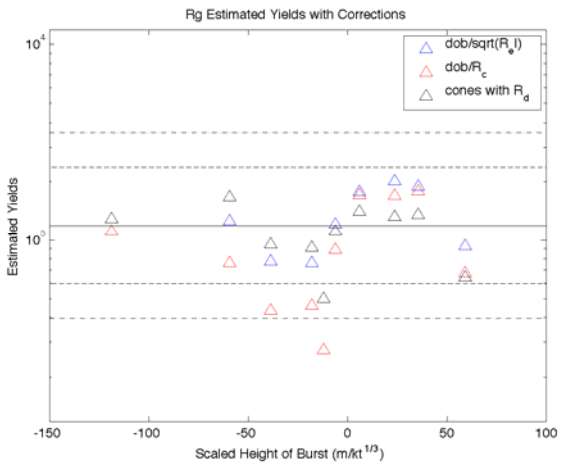

Figure 9. Estimated yields for the 1450-lb ANFO (1189-lb TNT equivalent) HUMBLE REDWOOD shots after correction for venting and cratering effects using correction factors based on phenomenological constraints such as elastic, cavity, and damage radii.

An underburied or above ground explosion typically creates a crater with a measurable radius, diameter, and volume. Crater parameters (Lenox et al., 2008) and permanent near-source surface displacements were obtained for the HUMBLE REDWOOD I explosions using digital photogrammetric techniques. We are currently in the process of deriving the crater parameters for the HRII explosions. Figure 10 shows the relationship between the estimated seismic moments based on *Rg* spectral amplitudes and the measured apparent crater volumes. There is a possible correlation between the crater volume and the drop in seismic moment with decreasing DOB.

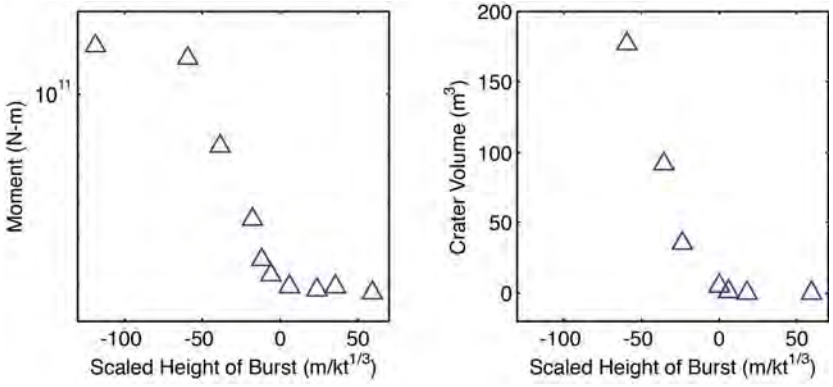

Figure 10. Relationship between estimated seismic moment (N-m) and crater volume (m^3) for the seven 1450-lb ANFO explosions detonated during HUMBLE REDWOOD I. In the coming months, we plan to measure the crater volumes of the three additional HRII explosions.

Time Domain Methods

We are also investigating a more simplistic time-domain approach in which we hope to use a formula(s) to estimate yield using measured *Rg* amplitudes. As an example of this method, Figure 11 shows peak *Rg* amplitudes bandpass-filtered between 0.5 and 2 Hz for seven different small explosions (108 – 365 lb TNT equivalent). All of the shots were fully contained and detonated in competent rock (e.g., not alluvium) with propagation in similar geologies as detonation. The only exception is the 100-lb C4 shot at GRABS (134 lb TNT equivalent) which propagated in limestone and granite until it crossed the Hubble Springs Fault Zone. As shown in Figure 11, this transition from rock to alluvium resulted in a sudden decrease in *Rg* amplitudes.

A *preliminary* formula that we have developed to predict 0.5 to 1 Hz *Rg* amplitudes (in cm/sec) from chemical explosions with yield (y in kg) is:

$$A_{Rg} = 0.06 \left(\frac{d}{y^{0.9}} \right)^{-1.4} \quad (5)$$

where d is distance in meters. We observed $y^{0.9}$ scaling similar to Adushkin (2001). After using these 7 small equations to develop Equation 5, we successfully validated the preliminary relationship using a ~5 ton Black Mesa SPE shot shown in Figure 11. More research is required as we plan to revise the formula for the frequency dependence of *Rg* above 2 Hz and to develop similar formulas for explosions in alluvium and other tectonic regimes.

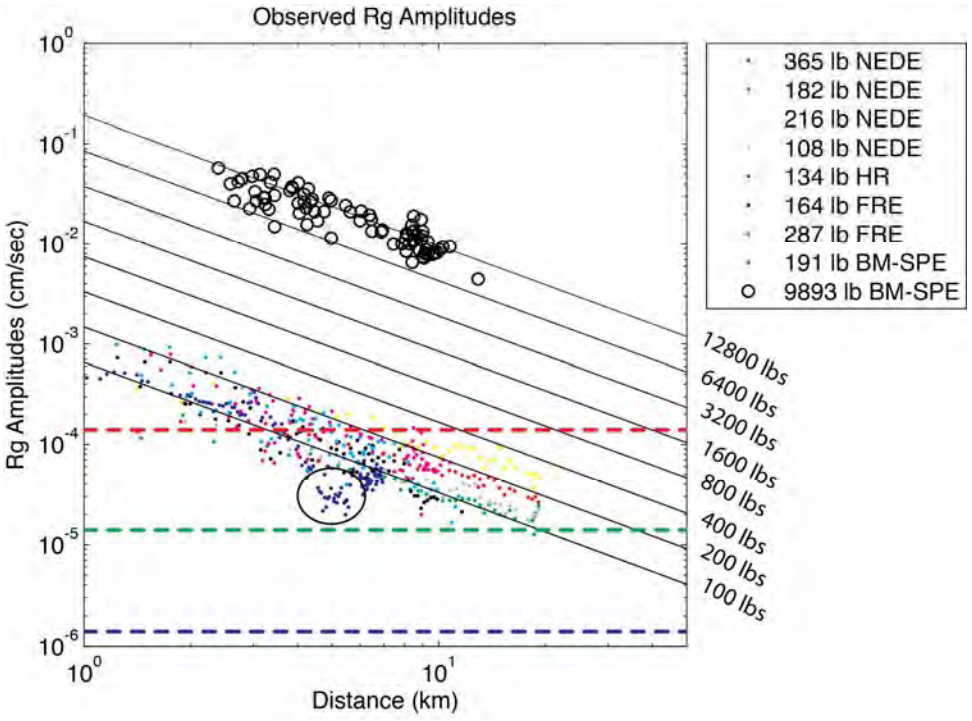

Figure 11. Time-domain 0.5-2 Hz *Rg* amplitude decay with distance for 7 small explosions (< 365 lbs) conducted in different lithologies. The slanted lines are predictions based on Equation 5. The dashed horizontal lines are typical noise levels including low noise (blue dashed), medium (green), and high (red). The circle is shown to note where propagation on the HR shot reaches the Hubbell Springs Fault (Figure 1) and transitions from limestone to alluvium. The explosions include ANFO, COMP-B, and C-4 types of explosives. NEDE=New England Damage Experiment; FRE=Frozen Rock Experiment; HR=HUMBLE REDWOOD; BM-SPE= Black Mesa Source Phenomenology Experiment. The largest shot (~5 ton BM-SPE shot) was our first attempt at validation of Equation 5. We plan to continue to test this new equation during the remainder of the contract.

CONCLUSIONS AND RECOMMENDATIONS

We have outlined a possible method for yield estimation using spectral amplitudes of *Rg*. The method includes model development, synthetic modeling and moment estimation, and conversion of the moment to yield. The method seems best suited for local monitoring in which several recordings of explosion are available in order to develop a velocity and attenuation model. The method is probably not applicable to sparse data at local and regional distances, although our time-domain formulas could be better suited for those applications. In the coming months, we plan to finish this pilot study by applying the spectral domain method to two additional datasets, testing and further development of the time-domain amplitude vs. yield formulas, and beginning to address the uncertainty in the yield estimates from *Rg*.

ACKNOWLEDGEMENTS

We thank Mark Leidig for development and maintenance of the databases used in this project. We thank Catherine Snelson for the refraction datasets collected for the HUMBLE REDWOOD experiments. Finally, we appreciate the assistance of Al Leverette, Jim Lewkowicz, and Bill Foxall for various aspects of this project.

REFERENCES

Adushkin, V. V. (2001). Yield estimation for Semipalatinsk underground nuclear explosions using seismic surface wave observations at near-regional distances, *Pure Appl. Geophys.* 158: 2217–2226.

Anderson, D. N., D. K. Fagan, M. A. Tinker, G. D. Kraft and K. D. Hutchenson (2007). A mathematical statistics formulation of the teleseismic explosion identification problem with multiple discriminants. *Bull. Seism. Soc. Am*. 97, 1730–1741.

Denny, M. D. and L. R. Johnson (1991). The explosion seismic source function: model and scaling laws revisited, in H. J. Patton and P. G. Richards, Eds., Explosion Source Phenomenology, *Geophysics Monograph* 65, *Am. Geophys. Union*, 1–24.

Dziewonski, A. M., S. Bloch, and N. Landisman, (1969). A technique for the analysis of transient seismic signals, *Bull. Seismol. Soc. Am.*, 59: 427–444,

Foxall, B. R., R. Reinke, C. Snelson, D. Seastrand, R. Marrs, O.R. Walton, and A.L. Ramirez (2008). The HUMBLE REDWOOD Seismic/acoustic coupling experiments, *Seismol. Res. Letts*, 79.

Foxall, B, R. Marrs, E. Lenox, R. Reinke, D. Seastrand, J. Bonner, K. Mayeda, and C. Snelson (2010). The HUMBLE REDWOOD seismic/acoustic coupling experiments. Joint inversion for yield using seismic, acoustic, and crater data. Abs. *Seismol. Res. Lett.* 81, No. 2 on page 315.

Grant, P. R., Jr. (1981). Geothermal potential on Kirtland Air Force Base lands, Bernalillo County, New Mexico, SAND81-7141 Contractor Report.

Herrin, E. T. and Goforth, T. T., (1977). Phase-matched filters: Application to the study of Rayleigh waves, *Bull. Seismol. Soc. Am,* 67, No. 1, 1259–75.

Herrmann, R. B. (2010). *Computer Programs in Seismology*, St. Louis University.

Hole, J. A. and B. C. Zelt, (1995). 3-D finite-difference reflection traveltimes. *Geophys. J. Int*., 121: 427–434.

Lenox, E. A., P. H. Thompson, and R. W. Henny (2008). Applicaton of photogrammetric techniques to crater measurements for shallow buried, surface, and small height of burst explosions. Proceedings of the MABS 20 (International Symposium on the Miltary Applications of Blast and Shock) Oslo, Norway, Sept, 2008.

Kafka, A. (1990). *Rg* as depth discriminant for earthquakes and explosions: a case study in New England, *Bull. Seismol. Soc. Am*, 80: 373–394.

Myers, S. C., W. R. Walter, K. Mayeda, and L. Glenn (1999). Observations in support of *Rg* scattering as a source for explosion *S* waves: regional and local recordings of the 1997 Kazakhstan depth of burial experiment, *Bull. Seismol. Soc. Am.* 89: 544–549.

Patton, H., J. Bonner, and I. Gupta, (2005). *Rg* excitation by underground explosions: insights from source modeling the 1997 Kazahkstan depth of burial experiments. *Geophys. J. Int.* doi:10.1111/j.1365-246X.2005.02752.x

Saikia, C. K., A. L. Kafka, S. C. Gnewuch, and J. W. McTigue (1990). Shear velocity and intrinsic Q structure of the shallow crust in southeastern New England from *Rg* wave dispersion, *J. Geophys. Res., B, Solid Earth and Planets*, 95 (6): 8527–8541.

Stump, B. W. (1987). Mathematical representation and physical interpretation of a contained chemical explosion in alluvium, *Bull. Seismol. Soc. Am.* 77: 1312–1325.